RSC Advances

PAPER

View Article Online
View Journal | View Issue

Cite this: *RSC Adv.*, 2021, **11**, 15663

Metal ion size profoundly affects H_3glyox chelate chemistry†

Neha Choudhary, [ab] Kendall E. Barrett, [c] Manja Kubeil, [d] Valery Radchenko, [be] Jonathan W. Engle, [c] Holger Stephan, [d] María de Guadalupe Jaraquemada-Peláez *[a] and Chris Orvig *[a]

The bisoxine hexadentate chelating ligand, H_3glyox was investigated for its affinity for Mn^{2+}, Cu^{2+} and Lu^{3+} ions; all three metal ions are relevant with applications in nuclear medicine and medicinal inorganic chemistry. The aqueous coordination chemistry and thermodynamic stability of all three metal complexes were thoroughly investigated by detailed DFT structure calculations and stability constant determination, by employing UV in-batch spectrophotometric titrations, giving pM values (pM = $-\log[M^{n+}]_{free}$ when $[M^{n+}] = 1$ μM, [L] = 10 μM at pH 7.4 and 25 °C) – pCu (25.2) > pLu (18.1) > pMn (12.0). DFT calculated structures revealed different geometries and coordination preferences of the three metal ions; notable was an inner sphere water molecule in the Mn^{2+} complex. H_3glyox labels $[^{52g}Mn]Mn^{2+}$, $[^{64}Cu]Cu^{2+}$ and $[^{177}Lu]Lu^{3+}$ at ambient conditions with apparent molar activities of 40 MBq μmol^{-1}, 500 MBq μmol^{-1} and 25 GBq μmol^{-1}, respectively. Collectively, these initial investigations provide insight into the effects of metal ion size and charge on the chelation with the hexadentate H_3glyox and indicate that further investigations of the Mn^{2+}–H_3glyox complex in $^{52g/55}$Mn-based bimodal imaging might be worthwhile.

Received 7th March 2021
Accepted 16th April 2021

DOI: 10.1039/d1ra01793d

rsc.li/rsc-advances

Introduction

The radiotracer principle was first described by George de Hevesy, who stated that radiopharmaceuticals are administered at such low molar masses that they can participate in biological processes and facilitate imaging, but they do not perturb native biochemistry.[1] Positron emission tomography (PET) relies on β^+ emission of radionuclides; the emitted β^+ collides with an electron leading to simultaneous emission of two γ-rays of 511 keV energy in opposite directions. This co-emission of two γ-rays leads to higher sensitivity and resolution of PET compared to single photon emission computed tomography (SPECT) which relies on the detection of unique emitted γ-rays in all directions. With the recent advent of advanced technologies in production and preparation of new radioisotopes, there is access to a large number of radiometals with varying physical (emission type and energies, half-lives) and chemical properties (oxidation state, metal hardness, size, coordination preferences) which can be harnessed for their applications in nuclear medicine.[2–4]

ImmunoPET has emerged as an attractive imaging modality in the last decade because of the high affinity and specificity of the antibodies and their longer plasma half-life.[5] Therefore, there has been burgeoning interest in longer-lived PET radiometals such as ^{89}Zr ($t_{1/2}$ = 78.4 h), ^{64}Cu ($t_{1/2}$ = 12.7 h) and ^{52g}Mn ($t_{1/2}$ = 5.6 d) which match better with the biological half-lives of antibodies.[6–10] Another advantage offered by manganese-based agents is their application for bimodal imaging using ^{55}Mn (high spin quantum number, S = 5/2) which exhibits great potential in Mn-based magnetic resonance imaging (MRI) contrast agents.[8,11,12] ^{64}Cu ($t_{1/2}$ = 12.7 h, $E\beta^+$ = 278 keV (19%), $E\beta^-$ = 190 keV (39%), EC (61%)) has been a radionuclide of great interest for five decades because of its unique decay scheme, which combines three types of decay (β^+, β^- and EC), and Auger electron emission with therapeutic potential.[13] While ^{52g}Mn and ^{64}Cu are two PET radiometals, ^{177}Lu ($t_{1/2}$ = 6.7 d) is a long lived radionuclide with its low energy β^- emission ($E\beta^-_{avg}$ = 134 keV, 100%) which makes it ideal for the treatment of small tumors using radiotherapy and the two useful γ-emissions ($E_{\gamma1}$ = 208 keV (10.41%) and $E_{\gamma2}$ = 113 keV (6.23%)) for SPECT imaging.[14] Lutathera ([^{177}Lu][Lu-DOTA-TATE]) is a recently FDA-approved ^{177}Lu-based-radiopharmaceutical for

[a]*Medicinal Inorganic Chemistry Group, Department of Chemistry, University of British Columbia, 2036 Main Mall, Vancouver, British Columbia, V6T 1Z1, Canada. E-mail: orvig@chem.ubc.ca; mdgjara@chem.ubc.ca*

[b]*Life Sciences Division, TRIUMF, 4004 Wesbrook Mall, Vancouver, British Columbia, V6T 2A3, Canada*

[c]*Department of Medical Physics, University of Wisconsin, 1111 Highland Avenue, Madison, WI 53711, USA*

[d]*Institute of Radiopharmaceutical Cancer Research, Helmholtz-Zentrum Dresden-Rossendorf, Bautzner Landstraße 400, D-01328 Dresden, Germany*

[e]*Department of Chemistry, University of British Columbia, 2036 Main Mall, Vancouver, British Columbia, V6T 1Z1, Canada*

† Electronic supplementary information (ESI) available: NMR spectra of compounds **1–4**, high resolution mass spectra, solution thermodynamic results, radiolabeling studies, density functional theory (DFT) calculations. See DOI: 10.1039/d1ra01793d

the treatment of somatostatin receptor positive gastroenteropancreatic neuroendocrine tumors.[15]

Previously, we reported a versatile bisoxine hexadentate chelator, H_3glyox (Chart 1); its metal complexes (Sc^{3+}, Ga^{3+} and In^{3+}) displayed excellent thermodynamic stability in solution and against *in vitro* human serum challenge.[16] Rapid radiolabeling of [^{44}Sc]Sc^{3+}, [^{68}Ga]Ga^{3+} and [^{111}In]In^{3+} at ambient conditions (RT, 15 min, pH 7) was observed with high specific activity and quantitative yields. Herein, we investigate the complexation ability of H_3glyox with the divalent metal ions (Mn^{2+} and Cu^{2+}) and trivalent metal ion (Lu^{3+}) to gauge the effect of metal ion size, oxidation state and varying coordination preferences on the sequestering capabilities of H_3glyox. All three metal ions (Mn^{2+}, Cu^{2+} and Lu^{3+}) are medicinally relevant but have very distinct chemical properties. Manganese and copper are first row transition metal ions with ionic radii of 0.83 Å (Mn^{2+}, CN 6, high spin) and 0.73 Å (Cu^{2+}, CN 6) respectively; while Lu^{3+} is the largest metal ion studied with H_3glyox with an ionic radius 0.86 Å (CN 6).[17] These results are compared with the previous study[16] to draw conclusions across the periodic table for the applicability of this unique ligand.

Results and discussion

Synthesis and characterisation

An easier modular higher yielding synthetic route is reported here for H_3glyox from commercially available starting materials (Scheme 1). The compound 2-(bromomethyl)quinolin-8-ol (**2**) was prepared in two steps which involved a reduction of the 8-hydroxyquinoline-2-aldehyde using $NaBH_4$ to give compound **1**, which was then brominated using PBr_3. This synthetic scheme provides a convenient method for the preparation of the alkylating compound **2** and overcomes the limitations of free radical bromination.[18,19] Another advantage offered by this synthetic route is that it makes possible functionalised derivatives of the ligand by using other amino acids such as *p*-NO_2–phenylalanine and *N*-alkylation using **2** in presence of base (K_2CO_3) and catalytic amount of KI. Compound **2** is not very stable at room temperature and is prone to decomposition; therefore, it is recommended to use it immediately. No additional column purification was required for the synthesis of compound **2** and the reactions provided high yields. H_3glyox was prepared in overall 90% yield by S_N2 reaction of glycine ethyl ester and compound **2** in basic conditions, and subsequent ethyl group deprotection under acidic conditions.

Metal complexes

Equimolar 1 : 1 concentration solutions of the ligand H_3glyox and the corresponding metal salts ($MnCl_2$, $CuSO_4$ and $Lu(NO_3)_3$) dissolved in water/D_2O were mixed together and the pH was adjusted to 7 using 0.1 M NaOH to give the metal complexes. LR-MS and HR-MS were used to confirm the formation of the complexes, along with the change in

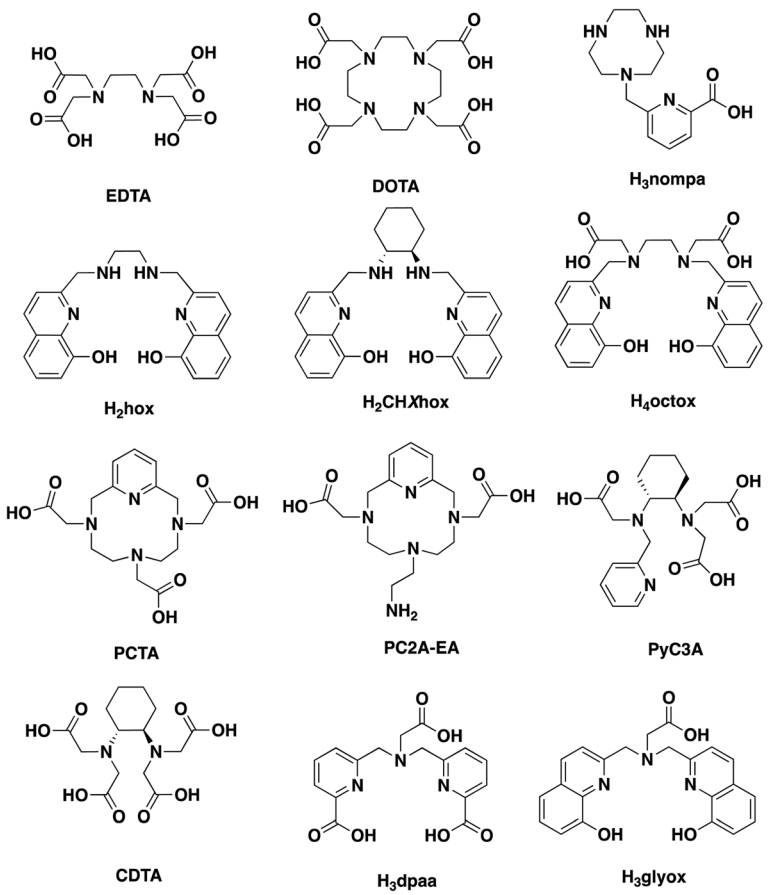

Chart 1 Structures of discussed chelators.

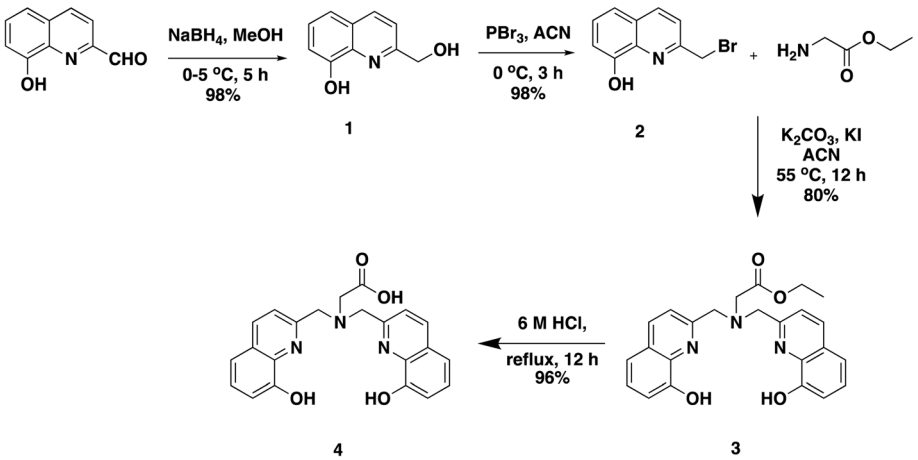

Scheme 1 Improved high yield modular synthetic scheme for H_3glyox, 4.

fluorescence of the ligand observed under UV light. The addition of $CuSO_4$ to the ligand solution led to the quenching of the fluorescence which was expected on Cu^{2+} complexation,[20] meanwhile no changes in fluorescence intensity were observed on addition of $MnCl_2$,[21] but there was a drastic increase in fluorescence intensity on complexation of Lu^{3+} ion. In Fig. 1, the changes in chemical shift of the protons of the ligand on complexation with Lu^{3+} ion can be noted in the ^{1}H NMR spectrum of the Lu^{3+}–H_3glyox complex but the complete coordination of Lu^{3+} ion remains inconclusive; there was no success in obtaining ^{13}C NMR or 2D NMR spectra due to the poor solubility of the complex, leading to precipitation over time. Comparing the ^{1}H NMR spectra of the Ga^{3+}–H_3glyox and Lu^{3+}–H_3glyox systems, it can be hypothesized that due to the larger

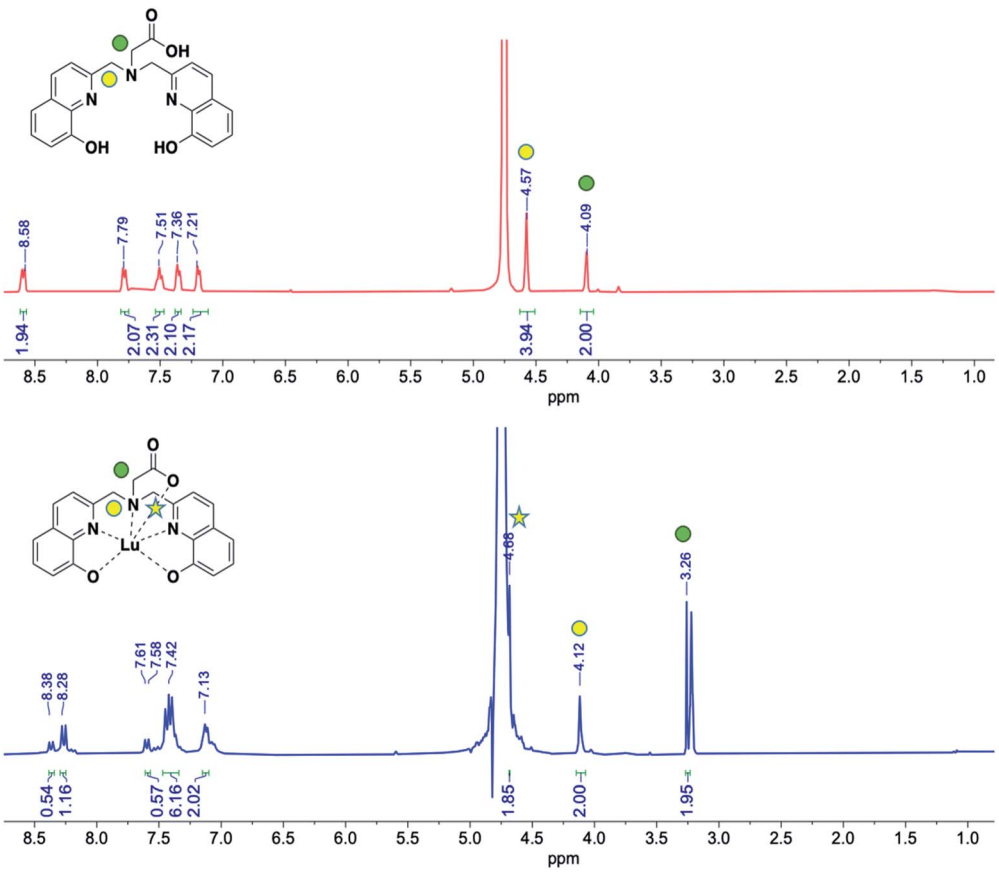

Fig. 1 ^{1}H NMR spectra (300 MHz, room temperature, D_2O, pD = 7) of the ligand H_3glyox (top in red) and the Lu^{3+}–H_3glyox complex (bottom in blue).

ionic size of Lu^{3+} (0.86 Å) as compared to smaller Ga^{3+} (0.62 Å) ion, the Lu^{3+} ion does not fit well in the cavity of the ligand and forms an asymmetric complex.[16]

Density functional theory calculations

In the absence of crystal structures for the Ga^{3+}, Mn^{2+}, Cu^{2+} and Lu^{3+} complexes, and inconclusive ^{1}H NMR of the Lu^{3+}–H_3glyox complex, DFT calculations were undertaken in order to study the coordination environment differences of the metal complexes in solution. The calculated structures are presented in Fig. 2 along with their coordination spheres. Fig. 2A demonstrates the distorted octahedral geometry (N_2O_4) around Ga^{3+} in the calculated structure of [Ga(glyox)(H_2O)], the two oxine arms bind Ga^{3+} in a slightly distorted plane with axial coordination from the carboxylic group and *trans* water molecule, analogous to the crystal structure of [Ga(dpaa)(H_2O)] without coordination of the tertiary N atom (Ga–N3 = 2.644 Å).[22] The average Ga–O(ox) bond distances are similar for the reported crystal structure of $[Ga(hox)]^+$ and the calculated structure of [Ga(glyox)(H_2O)] with average bond distances of 1.959 Å and 2.000 Å, respectively.[23] Meanwhile, the calculated average Ga–N(ox) bond distances in [Ga(glyox)(H_2O)], are slightly longer than in $[Ga(hox)]^+$ with a difference of 0.257 Å.[23]

The calculated structure in Fig. 2B reveals that the geometry around Mn^{2+} is distorted octahedral with five donor atoms of the ligand and an additional O-donor atom of a water molecule. On comparing bond distances in the calculation of $[Mn(glyox)(H_2O)]^-$ with those in the reported crystal structure of [Sc(glyox)(H_2O)],[16] it is noted that the average Mn–O(ox) and Mn–N(ox) bond distances are slightly shorter in $[Mn(glyox)(H_2O)]^-$ with an average bond distance of 2.067 Å and 2.180 Å, respectively, despite the bigger size of Mn^{2+} (0.83 Å, CN 6)[17] *vs.* Sc^{3+} (0.74 Å, CN 6).[17] The bond distance of the amine Mn–N3 is somewhat longer (2.764 Å) than the analogous amine Sc–N (2.515 Å); the former is not considered as a coordinated donor atom.[16] Additionally, comparison of the calculated structure of $[Mn(glyox)(H_2O)]^-$ with the reported crystal structure of analogous $[Mn(dpaa)(H_2O)]^-$ complex[24] reveals that the average Mn–O(ox) and Mn–N(ox) bond distances are shorter than the Mn–O(pa) and Mn–N(pa) bond distances with a difference of 0.199 Å and 0.079 Å, respectively.[24] It is noteworthy that the DFT calculated structures for both $[Mn(glyox)(H_2O)]^-$ and $[Mn(dpaa)(H_2O)]^-$ consist of an additional water molecule coordinated to the metal centre.[32]

Cu^{2+} prefers five-fold coordination with H_3glyox, leading to a distorted square pyramidal geometry (Fig. 2C), in which the donor atoms N1, O1, O2 and O3 define the basal plane and the

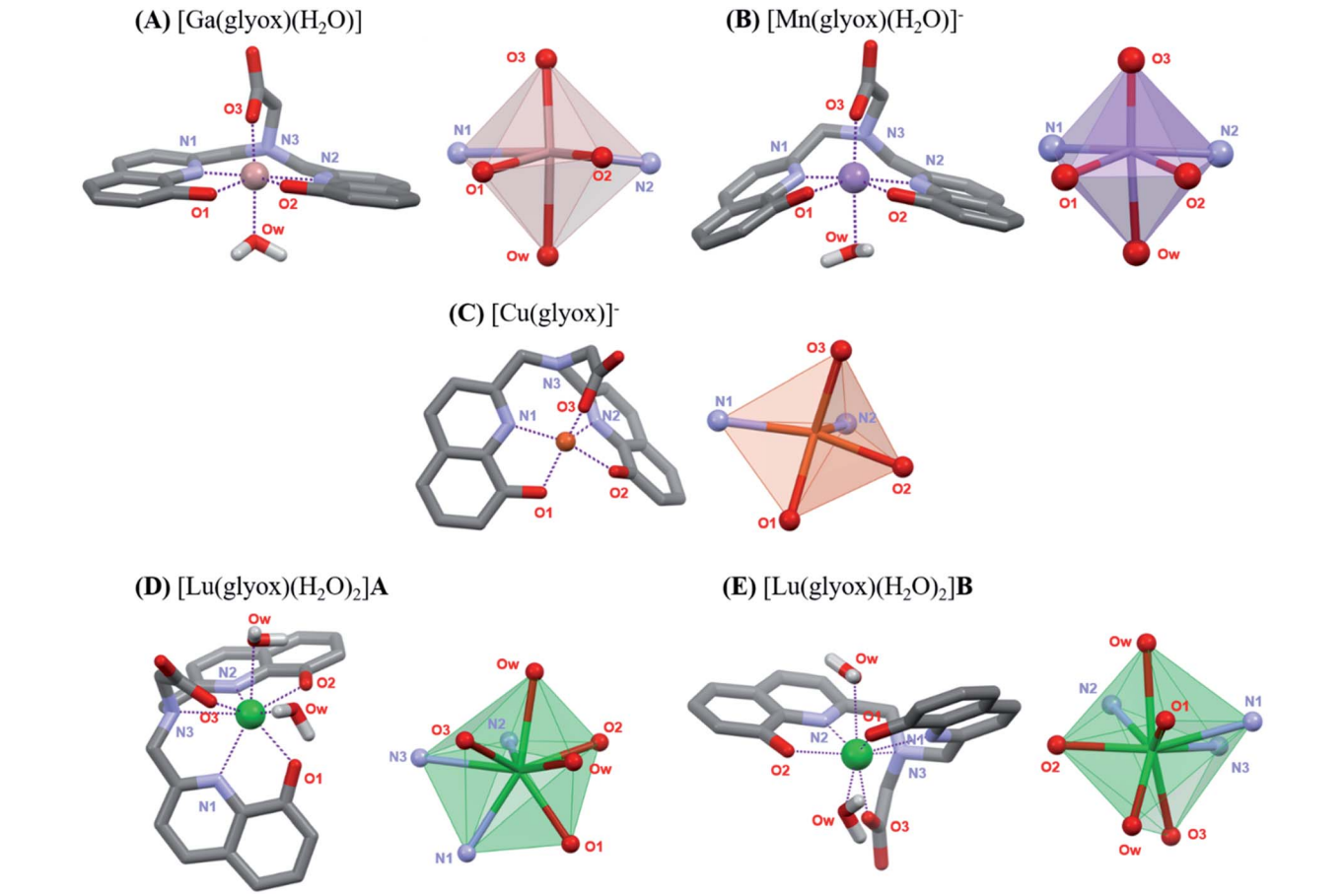

Fig. 2 DFT calculated structures of (A) [Ga(glyox)(H_2O)], (B) $[Mn(glyox)(H_2O)]^-$, (C) $[Cu(glyox)]^-$, (D) $[Lu(glyox)(H_2O)_2]$**A** and (E) $[Lu(glyox)(H_2O)_2]$**B**; bond distances are found in Tables S5 and S6.†

apical position is occupied by the N2 atom of the oxine arm. The inclusion of either one or three explicit water molecules in the calculations did not converge to a six-coordinate environment in either case (Fig. S17 and S18†). It has been previously reported that solvated Cu^{2+} ion prefers penta-coordination *vs.* the general assumption of octahedral solvation.[25] Similarly, Cu^{2+} complexes of monopicolinate derivatives of cyclen and cyclam, and $[Cu(nompa)]^+$ (Chart 1) all exhibit five-coordinate Cu^{2+} ion.[26,27] Table S5† presents the calculated bond distances from the DFT structures. Compared to the Cu–O(ox) bond distance of 2.142 Å in the reported [Cu(hox)] structure,[28] the Cu–O(ox) bond is slightly shorter in $[Cu(glyox)]^-$ complex with an average Cu–O(ox) bond distance of 2.006 Å. Due to the strong affinity of Cu^{2+} for the 8-hydroxyquinoline scaffold, the coordination uses the N_2O_2 donor set of the two oxine arms of the ligand and the O atom of the carboxylic group. The preorganization and rigidity of H_3glyox leads to the longer distances for the coordination of the amine N-atom and this is reflected in the long Cu–N3 bond distance of 2.781 Å which is not considered as coordinated.

Fig. 2D and E illustrates the two geometrical isomers for $[Lu(glyox)(H_2O)_2]$ (*cis*- and *trans*-diaqua) obtained through DFT calculations and the two structures exhibit a small energy difference ($\Delta G = 3.85$ kJ mol^{-1}); bond distances are tabulated in Table S6.† As expected, Lu^{3+} forms an eight-coordinate complex with the hexadentate glyox^{3-} and two water molecules, in agreement with the reported crystal structure of the analogous $[Lu(dpaa)(H_2O)_2]$ complex.[29] There are no significant differences in the bond lengths for the calculated *cis* $[Lu(glyox)(H_2O)_2]$ complex (Fig. 2D) and crystal structure of $[Lu(dpaa)(H_2O)_2]$. The calculated mean bond distances for Lu–O_{ox} and Lu–N_{ox} in *cis* $[Lu(glyox)(H_2O)_2]$ are 2.256 Å and 2.431 Å, respectively; compared to the mean bond distances of 2.576 Å and 2.398 Å reported for Lu–O_{pa} and Lu–N_{pa} in $[Lu(dpaa)(H_2O)_2]$ crystal structure.[29] Due to the rigid and distorted planar structure of the ligand,[16] the largest of the three metal ions studied here, Lu^{3+}, is exposed to coordination from solvent molecules. Hence, a lesser kinetic inertness of the Lu^{3+}–H_3glyox complex can be predicted from the incorporation of the two *cis* or *trans* water molecules completing the Lu^{3+}–H_3glyox coordination sphere.

Solution thermodynamics

The evaluation of a chelator for its use in radiometal-based radiopharmaceuticals heavily relies on the determination of the thermodynamic formation constant (log K_{ML}) for the metal complex and the protonation constants of H_3glyox (Table 1).[16] Herein, the aim was to determine the thermodynamic stability of the M^{n+}–H_3glyox complexes ($M^{n+} = Mn^{2+}$, Cu^{2+} and Lu^{3+}). UV in-batch spectrophotometric titrations were applied to determine the stability constants and the results from the equilibrium studies are summarised in Table 2. Aqueous solutions of equimolar concentrations of H_3glyox and each of three different metal ions were prepared at varying pH using standardised HCl and NaOH solutions, and were allowed to reach equilibrium before measuring the UV-spectra.

On comparing the extensive spectral changes in the electronic spectra of the metal complexes with the spectra of the ligand,[16] the complexation is observed directly (Fig. S9–S11†). The stability constants of the metal complexes were determined using HypSpec2014 (ref. 30) by analysing the experimental data along with the molar absorptivity of the different protonated species of $H_x$glyox (Table 1).[16] The speciation plots for the Mn^{2+}–H_3glyox, Cu^{2+}–H_3glyox, and Lu^{3+}–H_3glyox systems are presented in Fig. 3. In the aqueous environment, there is always competition between protons (H^+) and the metal ions (M^{n+}) for the basic donor atoms of the ligands. Therefore, the pM value[31] (pM $= -\log[M^{n+}]_{free}$ where $[M^{n+}] = 1$ μM, $[L] = 10$ μM at pH = 7.4) is a reliable thermodynamic parameter to evaluate the sequestrating ability of the ligand for a specific metal ion at physiological pH and allows for a better comparison of the affinity of different ligands with different denticities, basicity and metal complex stoichiometries for a specific metal ion.

For the Mn^{2+}–H_3glyox system, the complex formation equilibria studies showed a trio of species Mn(Hglyox), $[Mn(glyox)]^-$ and $[Mn(glyox)(OH)]^{2-}$. The complexation begins around pH 3.5 from the free $[Mn(H_2O)_6]^{2+}$ to form the monoprotonated Mn(Hglyox) complex. Around pH 5, the formation of the $[Mn(glyox)]^-$ species can be observed as there is an increase in the absorbance bands at $\lambda_{max} = 255$ and 370 nm characteristic of quinolinate metal complexes.[16,23,32] The formation of the metal-hydroxo species $[Mn(glyox)(OH)]^{2-}$ starts after pH 8 and predominates at basic pH without the presence of free metal in solution (Fig. S9†). The absorbance band with $\lambda_{max} = 255$ nm (Fig. S9C†) demonstrates the complexation of Mn^{2+} by the ligand in a manner similar to the UV-Vis spectrum for $Mn(oxinate)_2$ complex formation.[8]

Consistent with the lack of ligand field stabilisation in the $3d^5$ configuration of Mn^{2+}, $[Mn(glyox)]^-$ is the least

Table 1 Stepwise protonation constants (log β) and protonation constants (log K) of H_3glyox at 25 °C (ref. 16)

Equilibrium reaction	log β^a	log K^a
$L^{3-} + H^+ \leftrightarrows HL^{2-}$	10.66(1)[b]	10.66(1)
$HL^{2-} + H^+ \leftrightarrows H_2L^-$	20.36(1)[b]	9.70(1)
$H_2L^- + H^+ \leftrightarrows H_3L$	27.87(2)[b]	7.51(2)
$H_3L + H^+ \leftrightarrows H_4L^+$	33.28(1)[b]	5.41(1)
$H_4L^+ + H^+ \leftrightarrows H_5L^{2+}$	36.61(1)[b]	3.33(1)
$H_5L^{2+} + H^+ \leftrightarrows H_6L^{3+}$	39.27(1)[b]	2.66(1)

[a] From ref. 16. [b] In-batch UV spectrophotometric titrations at $I = 0.16$ M NaCl.

Table 2 Stability constants (log K_{pqr}) and corresponding stepwise protonation constants log K_{1q1} (MH_qL)[a] of H_3glyox complexes with Mn^{2+}, Cu^{2+} and Lu^{3+} ($T = 25$ °C, $I = 0.16$ M NaCl)

	Mn^{2+}	Cu^{2+}	Lu^{3+}
log K_{101} (ML)	16.75(1)	30.20 (1)	23.04(1)
log K_{111} (MHL)	7.17(1)	3.90 (1)	4.30(1)
log K_{1-11} (M(OH)L)	10.45(2)	8.98 (1)	8.74(1)
pM[b]	**12.0**	**25.2**	**18.1**

[a] $K_{1q1} = [MH_qL]/[MH_{q-1}L][H]_q$; $(q-1) = -1$ denotes OH. [b] pM[31] defined as $-\log[M^{n+}]_{free}$ when $[M^{n+}] = 1$ μM and $[L] = 10$ μM at pH 7.4.

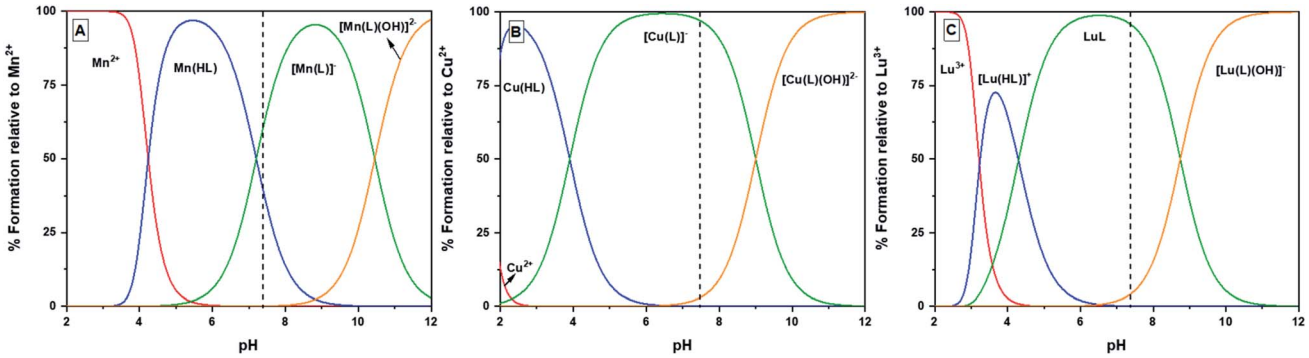

Fig. 3 Speciation diagrams of the M^{n+}–H_3glyox complexes where M^{n+} = Mn^{2+}, Cu^{2+} and Lu^{3+}; dashed line indicates pH 7.4.

Table 3 Stability constants (log K_{ML}), corresponding stepwise protonation constants (log K_{MHL}) and pMn values[33] of relevant Mn^{2+} chelators

Chelator	H_3glyox[a]	H_3dpaa[b]	PyC3A[c]	PC2A-EA[d]	PCTA[d]
log K_{ML}	16.75(1)	13.19(5)	14.14	19.01	16.83
log K_{MHL}	7.17(1)	2.90(6)	2.43	6.88	1.96
log $K_{M(OH)L}$	10.45(2)	11.97(6)	—	—	—
pMn[e]	**8.03**	**8.98**	**8.17**	**9.27**	**9.74**

[a] This work. [b] From ref. 24. [c] From ref. 11. [d] From ref. 34. [e] pMn[33] defined as $-\log[Mn^{2+}]_{free}$ when $[Mn^{2+}] = [L] = 10$ μM at pH 7.4.

thermodynamically stable metal complex of H_3glyox among all six metal ions studied.[16] But on the comparison (Table 3) with other macrocyclic and non-macrocyclic aminopolycarboxylate chelators (Chart 1) studied for Mn^{2+} complexation, and in particular, with the highest pMn reported for the macrocycle PCTA, H_3glyox has a pMn value[33] (pMn = $-\log[Mn^{n+}]_{free}$ when $[Mn^{n+}] = [L] = 10$ μM at pH 7.4, unique pMn conditions different than for pM above with all other metal ions) just 1.71 units lower, notwithstanding having both nearly the same thermodynamic stability (log K_{ML} = 16.75(1) for H_3glyox and log K_{ML} = 16.83 for PCTA).[34] On the other hand, the log K_{MnL} value for $[Mn(glyox)]^-$ is 3.56 units higher than for the structurally analogous $[Mn(dpaa)]^-$ which indeed reflects the effect of the oxine *vs.* picolinic acid groups on complexation of Mn^{2+} ion.[24] In Fig. 4B, pMn[31] (pMn = $-\log[Mn^{n+}]_{free}$ when $[Mn^{n+}] = 1$ μM; [L] = 10 μM at pH 7.4) *vs.* pH are plotted for the most relevant Mn chelators to demonstrate the effect of the overall basicity of the ligand on the metal scavenging ability at different pH. The most significant effect can be observed at physiological pH where, even though the stability constant of $[Mn(glyox)]^-$ (log K_{ML} = 16.75) stands within the highest reported (Tables 3 and S7†), the high overall basicity of H_3glyox with respect to the other ligands (Table S7†), mainly imparted by the two basic oxine–OH in the arms, makes the competition higher at physiological pH and consequently, lowers the conditional stability. Nevertheless, we see that still at higher pH the pMn continues to increase as the metal is secured by the $[Mn(glyox)(OH)]^{2-}$ species which reaches its maxima at pH ~12. Additionally, since the pH-dependent Mn^{2+} scavenging profile is very close (and even superior at higher pH) to that of the also non-macrocyclic chelator PyC3A,[11] it is worth to further explore the potential of this ligand for Mn^{2+} medicinal applications.

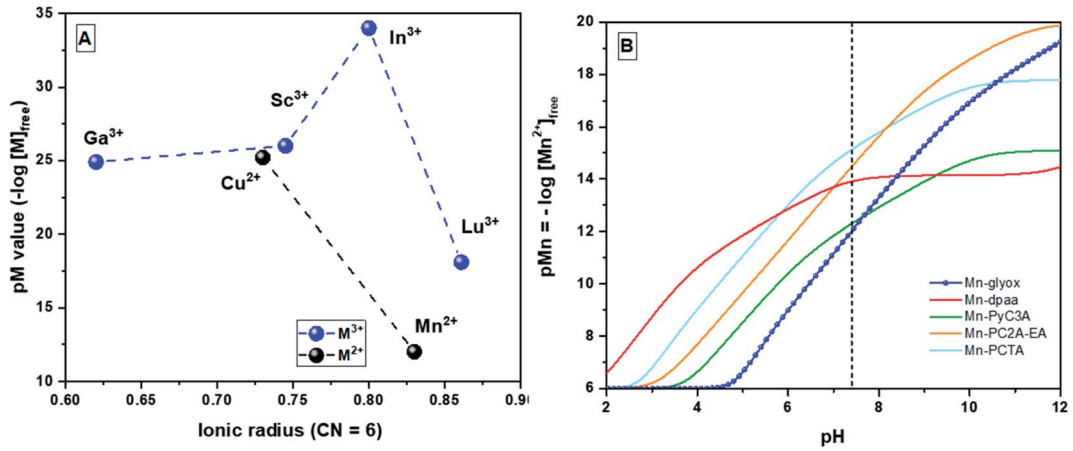

Fig. 4 (A) pM values[31] *vs.* ionic radii[17] for M^{n+}–H_3glyox complexes (n = 2 and 3) (CN = 6), pM = $-\log[M^{n+}]_{free}$ when $[M^{n+}] = 1$ μM and [L] = 10 μM at pH 7.4; (B) Mn^{2+} scavenging ability of different chelators as the pH is raised from 2 to 12, when $[Mn^{2+}] = 1$ μM and [L] = 10 μM;[31] dashed line represents physiological pH 7.4.

For each of the Cu^{2+}–H_3glyox and Lu^{3+}–H_3glyox systems, three metal–ligand species were observed (Fig. 3) – the protonated metal complex, Cu(Hglyox) and $[Lu(Hglyox)]^+$, the metal complex, $[Cu(glyox)]^-$ and Lu(glyox), and the hydroxo–metal complex, $[Cu(glyox)(OH)]^{2-}$ and $[Lu(glyox)(OH)]^-$. At neutral pH 7, the binary metal complexes $[Cu(glyox)]^-$ and Lu(glyox) are completely formed.

For the Cu^{2+}–H_3glyox system, different isosbestic points (Fig. S10†) can be seen in both the regions (225–300 nm and 300–450 nm) of the spectra with the increase in pH from 0.37 to 11.07 which indicates presence of different metal complex species in equilibrium. On comparing pM values of the Cu^{2+} complexes of H_3glyox, H_2hox and H_2*CHX*hox, all belonging to the same "ox" family with varying backbone, they follow the trend $[Cu(glyox)]^-$ (pCu = 25.2, $\log K_{ML} = 30.30$) > Cu(*CHX*hox) (pCu = 23.9, $\log K_{ML} = 29.78$) > Cu(hox) (pCu = 22.8, $\log K_{ML} = 22.80$).[28] This comparison demonstrates that the pre-organisation of the ligand leads to stronger complexation of Cu^{2+}.

For the Lu^{3+}–H_3glyox complexation equilibria, as pH increases from 3.74 to 6.54, there is an increase in absorption spectra at $\lambda_{max} = 260$ nm with new isosbestic points at $\lambda = 252$, 338 nm (Fig. S11†). Although both H_3glyox (hexadentate) and H_4octox (octadentate) differ in their denticity, they have quite similar affinities for Lu^{3+}; pM = 18.1 for Lu(glyox) and pM = 18.2 for $[Lu(octox)]^-$ and the stability constants ($\log K_{ML}$) are 23.04 and 24.66, respectively.[32]

Fig. 4A summarizes the effects of the metal ion size and charge on chelation with H_3glyox. As reported, the medium sized trivalent metal ions (Sc^{3+}, Ga^{3+} and In^{3+}) form thermodynamically stable and transchelation-resistant charge neutral complexes.[16] Meanwhile, the larger trivalent lanthanide, Lu^{3+} is a poor match for the H_3glox cavity size compared to the other smaller metals. Both the divalent metal ions Mn^{2+} and Cu^{2+}, however, form thermodynamically stable complexes ($\log K_{MnL} = 16.75$ and $\log K_{CuL} = 30.21$) which suggested that radiolabeling studies might be rewarding.

Radiolabeling with $[^{64}Cu]CuCl_2$

Preliminary radiolabeling experiments were done in order to determine the complexation kinetics and radiolabeling efficiency of H_3glyox with $[^{64}Cu]CuCl_2$. The first set of experiments involved radiolabeling in various buffer solutions (0.1 M MES, 0.1 M NH_4OAc and 0.1 M NaOAc) at pH 5.5 and 6; quantitative radiolabeling (RCY > 95%) was achieved in both 0.1 M MES and 0.1 M NaOAc within 15 minutes at pH 6 and $[L] = 10^{-5}$ M with the apparent molar activity of 500 MBq μmol^{-1}. The second set of experiments varied temperature and reaction time *vs.* radiolabeling efficiency. No significant changes in radiolabeling efficiency were observed when radiolabeling with $[^{64}Cu]CuCl_2$ was done at room temperature, 37 °C and 80 °C, while the radiochemical yields (RCY) observed for the time dependent reactions are summarised in Table 4. Further, the ligand solution concentration was varied to determine the ligand concentration dependant radiolabeling efficiency, $[H_3glyox] = 10^{-4}$ to 10^{-7} M and the results are summarised in Table 5. The radiochemical yields were obtained by integrating the area under the peaks observed for TLC (Fig. S13†) when eluted with 0.1 M EDTA (pH 5) ($[^{64}Cu][Cu(glyox)]^-$, $R_f < 0.1$; $[^{64}Cu]$Cu-EDTA, $R_f > 0.7$), consistent with the well-resolved peaks in the HPLC trace (Fig. S12†). Although H_3glyox labels copper-64 at ambient conditions, it was found that the $[^{64}Cu(glyox)]^-$ complex is unstable under acidic conditions (0.1% TFA in MQ water) as seen in the radio-HPLC trace. This is consistent with the observations and inferences made from both DFT calculations and solution studies due the protonation of the carboxylate arm at pH below 5.

Radiolabeling with $[^{52}Mn]MnCl_2$

A radiochemically isolated $[^{52g}Mn]Mn^{2+}$ sample[35] was titrated against varying concentrations of H_3glyox (0–100 000 ng mL^{-1}) yielding apparent molar activities of 30 MBq μmol^{-1} at pH 6.5 and 40 MBq μmol^{-1} at pH 7. The labelling of $[^{52g}Mn]Mn^{2+}$ by H_3glyox was compared with the "gold standard" chelator – DOTA at similar conditions (30 min, 85 °C, pH 7) and it was found that DOTA yields apparent molar activity of 60 MBq μmol^{-1}, slightly higher than that for $[^{52g}Mn]Mn^{2+}$–H_3glyox (40 MBq μmol^{-1}). It was observed that the molar activity of $[^{52g}Mn]Mn^{2+}$–H_3glyox increased with the use of higher activity of $[^{52g}Mn]Mn^{2+}$ per reaction. Radiolabeling was not attempted at pH > 7 to avoid hydrolysis of the Mn^{2+} ion. The radiochemical yields (RCY%) of chelated $[^{52g}Mn]Mn^{2+}$ were determined *via* TLC (silica gel plates) eluted with 0.1 M sodium citrate (Fig. S14†). The "free" $[^{52g}Mn]Mn^{2+}$ travels up the plate as $[^{52g}Mn]Mn^{2+}$–citrate complex ($R_f > 0.8$) while the $[^{52g}Mn]Mn^{2+}$–DOTA and $[^{52g}Mn]Mn^{2+}$–H_3glyox complex stayed at baseline ($R_f < 0.1$). It has been noted previously that a rigid scaffold such as bispidine around the Mn^{2+} ion endows the manganese complex with increased kinetic inertness and similar to

Table 4 Radiochemical yields *vs.* time for the copper-64 complex of H_3glyox ($n = 3$)

Time (min)	$[^{64}Cu]Cu^{2+}$ RCY[a] (%)
10	<60
20	100
40	100
60	100

[a] Room temperature, 0.1 M NaOAc/AcOH, pH 6, $[H_3glyox] = 10^{-5}$ M, 25 MBq $[^{64}Cu]CuCl_2$ per reaction.

Table 5 Radiochemical yields *vs.* concentration for the copper-64 complex of H_3glyox ($n = 3$)

[Ligand] (M)	$[^{64}Cu]Cu^{2+}$ RCY[a] (%)
10^{-4}	100
10^{-5}	100
10^{-6}	>95
10^{-7}	<10

[a] Room temperature, 0.1 M NaOAc/AcOH, pH 6, 15 min, 25 MBq $[^{64}Cu]CuCl_2$ per reaction.

Table 6 Radiolabeling data for the $[^{177}Lu]Lu^{3+}$–H_3glyox complex

Buffer	Time (min)	RCY[a] (%)
0.1 M NaOAc pH 7.0	15	75
0.1 M NaOAc pH 8.5	15	70
0.1 M NaOAc pH 7.0	30	80
0.1 M NaOAc pH 8.5	30	60

[a] Room temperature, [L] = 10^{-5} M, 2 MBq $[^{177}Lu]LuCl_3$ per reaction.

H_3glyox, the radiolabeling of $[^{52g}Mn]Mn^{2+}$ with a bispidine-based ligand was done at pH 7, 70 °C and 1 h.[36] Meanwhile, radiolabeling of $[^{52g}Mn]Mn^{2+}$ with the open chain chelator, CDTA (*trans*-1,2-diamino-cyclohexane-*N*,*N*,*N*′,*N*′-tetraacetic acid) is reported to be performed at pH 6, room temperature and 30 minutes ([CDTA] = 64 mM, ~8 MBq $[^{52g}Mn]MnCl_2$).[10] No data on apparent molar activities for ^{52g}Mn-labeled complexes were found in the literature for other chelators discussed here for comparison.[10,36]

Radiolabeling with $[^{177}Lu]LuCl_3$

Encouraged by the relatively high pM value (pLu = 18.1), preliminary radiolabeling studies were done to investigate the complexation kinetics of the hexadentate chelator H_3glyox with $[^{177}Lu]LuCl_3$. Although Lu^{3+} ion is a larger trivalent metal ion with an ionic radius of 86–103 pm and coordination number 6–9,[17] the mismatch with the cavity size of H_3glyox is evident from the observed RCYs. Table 6 summarizes the RCYs ($n = 3$) and as expected, quantitative radiolabeling (RCY > 95%) was not achieved even by varying conditions – pH 7.0 and 8.5 at 15 and 30 minutes. The decrease in RCY was observed when the labelling was performed at pH 8.5 after 30 minutes compared to the RCY at 15 minutes, this can be attributed to the labile nature of the $[^{177}Lu]Lu^{3+}$–H_3glyox complex and subsequent transchelation of Lu^{3+} ion by EDTA (pH 7, mobile phase) leading to lower RCYs. The radiochemical yields were determined by integrating the area under the peaks observed in the iTLC plates (Fig. S15,† $[^{177}Lu]Lu$(glyox), R_f < 0.1; $[^{177}Lu]Lu$(EDTA), R_f > 0.8). A high apparent molar activity of 25 GBq μmol^{-1} was achieved by using 10^{-6} M ligand concentration at ambient conditions (15 min, RT, and pH 7).

Conclusions

It has been an ongoing challenge for the medicinal inorganic chemistry community to stabilize the labile coordination complexes of endogenous metal ions such Mn^{2+} and Cu^{2+} in relevant biological environments. These results indicate that further investigation of the preorganized H_3glyox as a potential chelator for $^{52g/55}$Mn-based dual MRI-PET tracer application is worthwhile, supported by the DFT calculated structure of $[Mn(glyox)(H_2O)]^-$ and efficient radiolabeling of $[^{52g}Mn]Mn^{2+}$. In-batch UV spectrophotometric titrations were conducted to access the thermodynamic stability of the metal complexes by determining the formation constants, speciation diagrams and the pM values, which are in the order pCu (25.2) > pLu (18.1) > pMn (12.0). Although the thermodynamic stability of the Cu^{2+}–H_3glyox complex is higher than that of the Mn^{2+} complex and in agreement with the Irving–William series, the $[^{64}Cu][Cu(glyox)]^-$ was found to decompose under mild acidic conditions due to the formation of a protonated Cu(Hglyox) species at pH < 5. However, radiolabeling of H_3glyox with $[^{52g}Mn]Mn^{2+}$, $[^{64}Cu]Cu^{2+}$ and $[^{177}Lu]Lu^{3+}$ yielded apparent molar activities of 40 MBq μmol^{-1}, 500 MBq μmol^{-1} and 25 GBq μmol^{-1}, respectively. DFT calculations of the structures of the three complexes revealed that the Mn^{2+} is hexacoordinated and is bound to a water molecule similar to the reported $[Mn(dpaa)(H_2O)]^-$ structure,[24] which makes the Mn^{2+}–H_3glyox complex potentially relevant to Mn-based contrast agents. Based on these interesting and encouraging preliminary studies, the next step would be detailed studies to determine the kinetic inertness, water exchange rate and relaxivity measurements for application of H_3glyox in Mn-based MRI contrast agents. Meanwhile, it can be concluded that the highly preorganized and rigid binding cavity of the ligand H_3glyox is suitable for neither the smaller Cu^{2+} nor the larger Lu^{3+} ion.

Experimental section

Materials and methods

All solvents and reagents were purchased from commercial suppliers (Sigma-Aldrich, TCI America, Fischer Scientific, Alfa Aesar) and were used as received. Reactions were monitored by TLC (MERCK Kieselgel 60 F254, aluminum sheet). Flash chromatography was performed using SilicaFlash F60 silica gel (40–63 μM particle size), RediSep R_f HP silica columns, and a CombiFlash R_f column machine. Water used was ultrapure (18.2 MΩ cm^{-1} at 25 °C, Milli-Q, Millipore, Billerica, MA).

^{1}H and ^{13}C NMR spectroscopy was performed using Bruker Avance 300 and Bruker AV III HD 400 MHz spectrometers. Chemical shifts (δ) are quoted in ppm relative to residual solvent peaks as appropriate; coupling constants (J) are provided in Hertz (Hz). ^{1}H NMR signals were designated as follows: s (singlet), d (doublet), t (triplet), q (quartet), quin (quintet), sxt (sextet), spt (septet), m (multiplet), or a combination of these, with br representing a broad signal. Low resolution ESI-MS was performed on a Waters 2965 HPLC-MS with the sample prepared in methanol or acetonitrile (ACN). Results are labeled with m/z (abundance percentage) values – $[M + X]^{\pm}$. High resolution ESI-MS was performed on a Waters/Micromass LCT TOF-MS with the sample prepared in methanol. Results are labeled with m/z (abundance percentage) values. Semi-preparative reverse phase high-performance liquid chromatography (HPLC) for H_3glyox was performed on a Phenomenex Synergi hydro-RP 80 A, 250 × 21.2 mm column connected to a Waters 600 controller, a Waters 2487 dual wavelength absorbance detector, and a Waters delta 600 pump. The HPLC solvents were (A) H_2O containing 0.1% trifluoroacetic acid (TFA) and (B) CH_3CN containing 0.1% TFA. Silica gel impregnated TLC plates (MERCK Kieselgel 60 F254, aluminum sheet) were used to analyse $[^{64}Cu]Cu^{2+}$ and $[^{177}Lu]Lu^{3+}$ radiolabeling reaction progress and the complex stability tests were counted on

a BioScan System 200 imaging scanner equipped with a BioScan Autochanger 1000. For the evaluation of [^{52g}Mn]Mn^{2+}, TLC plates were scanned on a Packard Cyclone™ phosphor-storage plate equipped with Opti-quant™ software. Linear extrapolation was used to determine the amount of chelator needed to complex 50% and 100% of [^{52g}Mn]Mn^{2+}.

[^{177}Lu]$LuCl_3$ was purchased from Isotope Technologies Garching (ITG). All the isotopes used were no-carrier added (n.c.a.). The production of [^{64}Cu]$CuCl_2$ was performed at a TR-Flex cyclotron from Advanced Cyclotron Systems Inc (ACSI, Canada) according to a reported procedure *via* ^{64}Ni(p,n)^{64}Cu nuclear reaction and module-assisted separation as described in detail recently.[37] No-carrier-added [^{52g}Mn]Mn^{2+} was produced by irradiation of a metallic chromium target of natural isotopic abundance (83.8% ^{52}Cr; 9.5% ^{53}Cr; 4.3% ^{50}Cr; and 2.4% ^{54}Cr) with 16 MeV protons as described previously in a report.[35] Deionized water was filtered through the PURELAB Ultra Mk2 system.

Synthesis and characterisation

2-(Hydroxymethyl)quinolin-8-ol (1). 8-Hydroxyquinoline-2-aldehyde (0.35 g, 2.05 mmol) was dissolved in 20 mL CH_3OH in a 100 mL round bottom flask and $NaBH_4$ (0.10 g, 2.66 mmol) was added gradually to the reaction flask which was placed in an ice bath and stirred constantly for 5 hours. The reaction progress was monitored using TLC ($R_f = 0.5$, stationary phase – silica gel and mobile phase – 1 : 1 EtOAc/hexane). On completion of reaction after 5 hours, the solvent was removed under vacuum and the crude solid was dissolved in 10 mL distilled water and the product was extracted using DCM (20 mL × 3). The combined organic layers were dried over anhydrous $MgSO_4$ and the solvent was removed under vacuum to give white solid product **1** (0.35 g, 2.00 mmol, 98%). ^{1}H NMR (300 MHz, CD_3OD, RT): δ 8.21 (d, $J = 8.5$ Hz, 1H), 7.54 (d, $J = 8.5$ Hz, 1H), 7.38 (m, 2H), 7.11 (d, $J = 7.1$ Hz, 1H), 4.90 (s, 2H). ^{13}C NMR (75 MHz, CD_3OD, RT): δ 158.8, 152.8, 137.6, 136.7, 128.3, 126.9, 118.9, 117.7, 110.9, 64.6. LR-ESI-MS calcd for $C_{10}H_9NO_2$: 175.2. Found: 176.3 $[M + H]^+$.

2-(Bromomethyl)quinolin-8-ol (2). Compound **1** (0.32 g, 1.82 mmol) was dissolved in 25 mL dry ACN in a 100 mL round bottom flask and placed on an ice bath. PBr_3 (0.19 mL, 2.00 mmol) was added dropwise with constant stirring to the reaction mixture which was left to stir. After 3 hours, TLC analysis ($R_f = 0.8$, stationary phase – silica gel and mobile phase – 1 : 1 EtOAc/hexane) indicated the completion of reaction. The reaction was quenched by addition of saturated Na_2CO_3 (30 mL) and the mixture was stirred for another 10 minutes. The reaction mixture was transferred to a separating flask and DCM (3 × 20 mL) was used to extract out the product. The organic layers were combined and dried over anhydrous $MgSO_4$ and the solvent was removed under vacuum to slightly yellow colored product **2** (0.40 g, 1.78 mmol, 98%). ^{1}H NMR (300 MHz, CD_3OD, RT): δ 8.17 (d, $J = 8.5$ Hz, 1H), 7.61 (d, $J = 8.5$ Hz, 1H), 7.49 (t, $J = 7.9$ Hz, 1H), 7.36 (d, $J = 9.4$ Hz, 1H), 7.22 (d, $J = 7.6$ Hz, 1H) 4.73 (s, 2H). ^{13}C NMR (75 MHz, CD_3OD, RT): δ 157.8, 151.7, 137.4, 127.9, 127.6, 124.1, 119.4, 118.2, 111.1, 64.9. LR-ESI-MS calcd for $C_{10}H_8{}^{79}BrNO$: 238.0. Found: 239.1 $[M + H]^+$.

Ethyl bis((8-hydroxyquinolin-2-yl)methyl)glycinate (3). Compound **2** (0.54 g, 2.26 mmol) was dissolved in 30 mL dry ACN and to this solution was added glycine ethyl ester (0.20 g, 1.43 mmol), excess K_2CO_3 (0.90 g, 6.51 mmol) and KI (0.37 g, 2.26 mmol). The mixture was refluxed overnight at 55 °C; the reaction was then quenched with distilled water (10 mL) and the product was extracted with DCM (3 × 25 mL). The solvent was removed under a vacuum to give crude **3**, which was then purified by column chromatography (eluted with a gradient of 100% hexane to 100% ethyl acetate) to afford **3** as an off-white solid (0.47 g, 1.14 mmol, 61%, $R_f = 0.50$ in 20% EtOAc in hexane). ^{1}H NMR (300 MHz, $CDCl_3$, RT): δ 8.11 (d, $J = 8.5$ Hz, 2H), 7.72 (d, $J = 8.5$ Hz, 2H), 7.41 (m, 2H), 7.31 (d, $J = 8.2$ Hz, 2H), 7.17 (d, $J = 7.5$ Hz, 2H), 4.19 (m, 6H), 2.03 (s, 2H), 1.27 (t, $J = 7.1$ Hz, 3H). ^{13}C NMR (75 MHz, $CDCl_3$, RT): δ 171.3, 160.6, 157.1, 145.3, 140.8, 136.5, 136.4, 134.1, 128.9, 128.8, 127.0, 125.8, 122.9, 122.2, 60.7, 60.3, 55.4, 14.4. LR-ESI-MS calcd for $C_{24}H_{23}N_3O_4$: 417.4. Found: 440.3 $[M + Na]^+$.

Bis((8-hydroxyquinolin-2-yl)methyl)glycine, H_3glyox (4). Compound **3** (0.47 g, 1.14 mmol) was dissolved in HCl (10 mL, 6 M) and refluxed overnight. The solution was then cooled and the solvent was evaporated under reduced pressure to give a yellow coloured solid product **4** (0.42 g, 1.09 mmol, 96%). The purity of compound **4** was confirmed by the presence of a single sharp peak in the HPLC trace (Fig. S19†) with $t_R = 12.1$ min (eluents: (A) 0.1% TFA in H_2O and (B) 0.1% TFA in ACN with a linear gradient 5% to 100% B for 25 min and flow rate set to 1 mL min^{-1}). ^{1}H NMR (300 MHz, RT, D_2O): δ 8.58 (d, $J = 7.7$ Hz, 2H), 7.79 (d, $J = 7.9$ Hz, 2H), 7.51 (t, $J = 7.2$ Hz, 2H), 7.36 (d, $J = 7.6$ Hz, 2H), 7.21 (d, $J = 6.7$, 2H), 4.57 (s, 4H), 4.09 (s, 2H). ^{13}C NMR (75 MHz, RT, D_2O): δ 176.1, 155.1, 150.4, 146.9, 146.6, 130.9, 128.8, 128.4, 122.3, 119.2, 117.0, 58.5, 57.3. HR-ESI-MS calcd for $C_{22}H_{19}N_3O_4$: 389.1400. Found: 390.1451 $[M + H]^+$. Anal. calcd for $[H_3glyox \cdot 2.8\ HCl \cdot 1.3\ CH_3OH]$: C, 52.49; H, 5.1; N, 7.88. Found: C, 52.48; H, 5.11; N, 7.93.

[^{nat}Lu(glyox)]. A ^{1}H NMR spectrum of Lu^{3+}–H_3glyox was obtained by mixing together 1 : 1 (L : M) solutions of ligand and $Lu(NO_3)_3$ prepared in D_2O (10 mM) and 0.1 M NaOD was added to increase the pD of the solution to 7. ^{1}H NMR (300 MHz, RT, D_2O): δ 8.38 (d, $J = 8.6$ Hz, 0.5H), 8.28 (d, $J = 8.6$ Hz, 1H), 7.61 (t, $J = 8.5$ Hz, 0.5H), 7.42 (t, $J = 8.4$ Hz, 6H), 7.13 (m, 2H), 4.68 (s, 2H), 4.12 (s, 2H), 3.26 (s, 2H). HR-ESI-MS calcd for $C_{22}H_{16}{}^{175}LuN_3O_4$: 561.0548. Found: 562.0546 $[M + H]^+$.

H[^{nat}Mn(Hglyox)]. H_3glyox (10 mg, 0.02 mmol) was dissolved in 1 mL of distilled water in a scintillation vial, and $MnCl_2 \cdot 4H_2O$ (3.95 mg, 0.02 mmol) was added, followed by pH adjustment to ~7 using 0.1 M NaOH. The solution was left to stir for 1 h, leading to the precipitation of the metal complex which was confirmed using LR-ESI MS. HR-ESI-MS calcd for $C_{22}H_{17}{}^{55}MnN_3O_4$: 442.0599. Found: 443.0601 $[M + H]^+$.

Na[^{nat}Cu(Hglyox)]. H_3glyox (10 mg, 0.02 mmol) was dissolved in 1 mL of distilled water in a scintillation vial, and $CuSO_4 \cdot 5H_2O$ (5.00 mg, 0.02 mmol) was added, followed by pH adjustment to ~7 using 0.1 M NaOH. The solution was left to stir for 1 h, leading to the dark green colored precipitate which was filtered

and collected. Formation of the metal complex was confirmed using LR-ESI MS as well as quenching of fluorescence under a UV lamp. HR-ESI-MS calcd for $C_{22}H_{17}{}^{63}CuN_3O_4$: 450.0515, Found: 473.0412 $[M + Na]^+$.

Radiolabeling

For concentration-dependent labeling of copper-64, different aliquots were added from the stock solution of H_3glyox (2 mg dissolved in 1 mL 0.1 M HCl and 2 mL MQ H_2O, $\sim 10^{-3}$ M), mixed with $[^{64}Cu]CuCl_2$ (25 MBq) and diluted to a final volume of 500 μL using 0.1 M NaOAc buffer solution (pH 6). After incubation for 15 min at RT, the radiolabeling yields were determined using iTLC (silica gel plates developed with aqueous 0.1 M EDTA solution, pH 5; $[^{64}Cu][Cu(glyox)]^-$, $R_f < 0.1$; $[^{64}Cu]$Cu–EDTA, $R_f > 0.7$). For labeling of lutetium-177, a total volume of 500 μL of the reaction mixture was obtained by addition of an aliquot from the ligand stock solution (10^{-5} M), $[^{177}Lu]LuCl_3$ (2 MBq) and 0.1 M NaOAc/HOAc buffer (pH 7, 8.5). The RCYs were obtained by spotting an aliquot from reaction mixture after 15 min and 30 min on a TLC plate (silica gel) and developing with aqueous EDTA solution (0.1 M, pH 7). The $[^{177}Lu]$Lu(glyox) complex stayed on the baseline ($R_f < 0.1$) while "free" $[^{177}Lu]Lu^{3+}$ travelled up the plate as $[^{177}Lu]Lu^{3+}$–EDTA complex ($R_f > 0.7$). For labeling with ^{52g}Mn, a reported procedure was followed.[35] In summary, 100 μL of chelator solution was added to 1 mL vials in varying concentrations (0–100 000 ng mL^{-1}) and 100 μL of $[^{52g}Mn]Mn^{2+}$ solution (~2.7 MBq) was added to each vial. Finally, the pH of the solution was adjusted to pH 7 with addition of 100–200 μL of 1 M HEPES/NaOH buffer (pH 7). It was observed that the molar activity of $[^{52g}Mn]Mn^{2+}$–H_3glyox complex increased with the use of higher activity of $[^{52g}Mn]Mn^{2+}$ per reaction. The apparent molar activity for $[^{52g}Mn]Mn^{2+}$–H_3glyox complex determined from titration of ^{52g}Mn solutions with H_3glyox can be expressed as twice the ratio of the ^{52g}Mn over moles of chelator required to chelate 50% of the $[^{52g}Mn]Mn^{2+}$. Radiolabeling was not attempted at pH > 7 in order to avoid hydrolysis of the Mn^{2+} ion. Vials were agitated, assayed and heated for 30 minutes at 85 °C. The percentage of chelated $[^{52g}Mn]Mn^{2+}$ was determined *via* TLC (silica gel plates; Fig. S14†) eluted with 0.1 M aqueous sodium citrate (pH 5.5). The "free" $[^{52g}Mn]Mn^{2+}$ travels up the plate as $[^{52g}Mn]Mn^{2+}$–citrate complex ($R_f > 0.8$) while the $[^{52g}Mn]Mn^{2+}$–DOTA and $[^{52g}Mn]Mn^{2+}$–H_3glyox complexes stayed at baseline ($R_f < 0.1$).

Solution thermodynamics

Metal stability constants were calculated from UV spectrophotometric titration data obtained using a Cary 60 UV-Vis spectrophotometer in the spectral range of 200–450 nm. The path length was 1 cm for all samples. Individual samples (5 mL) containing the ligand (H_3glyox, $[L] = 2.5 \times 10^{-5}$ M) and the corresponding metal complexes ($M = Mn^{2+}$, Cu^{2+} and Lu^{3+}; $[ML] = 2.5 \times 10^{-5}$ M) were prepared in MQ water by adjusting the pH using standardized HCl or NaOH solutions, and NaCl was added to maintain a constant 0.16 M ionic strength over the pH range ~0.37–11.07. A Ross combination pH electrode was calibrated for hydrogen ion concentration using HCl as described before[38] and the results were analysed by the Gran[39] procedure. For the most acidic samples, the equilibrium H^+ concentration was calculated from solution stoichiometry and was not measured with the glass electrode. For the samples containing the metal complexes, the measurements were performed only when equilibrium was achieved. The stability constants for the metal complexes were calculated from the experimental data using the HypSpec2014 program.[30] Proton dissociation constants corresponding to hydrolysis of Mn^{2+}, Cu^{2+}, and Lu^{3+} aqueous ions included in the calculations were taken from Baes and Mesmer.[40] The species formed in the studied systems are characterized by the general equilibrium in eqn (1).

$$pM + qH + rL \leftrightarrow MpHqLr \text{ (charges omitted)} \quad (1)$$

By convention, a complex containing a metal ion M, proton H, and ligand L has the general formula MpHqLr. The stoichiometric index p might also be 0 in the case of ligand protonation equilibria, and negative values of q refer to proton removal or hydroxide ion addition during formation of the complex. The overall equilibrium constant for the formation of the complexes MpHqLr from its components is designated as log β. Stepwise equilibrium constants log K correspond to the difference in log units between the overall constants of sequentially protonated (or hydroxide) species. pM value is defined as $-\log[M^{n+}]_{free}$ calculated at specific conditions ($[M^{n+}] = 1$ μM, $[L^{x-}] = 10$ μM, pH 7.4)[31] except where pMn values amongst ligands are compared ($[Mn^{2+}] = 10$ μM, $[L^{x-}] = 10$ μM, pH 7.4).[33]

DFT calculations

All DFT simulations were performed as implemented in the Gaussian 16 revision c01.[41] Each structure was optimised and free energies were calculated using DFT with the hybrid meta generalized gradient approximation with the TPSSh exchange-correlation functional[42] and the def2-TZVP basis set[43] for all non-metal atoms. Effective core potentials (ECPs) were used to account for scalar relativistic effects in metal core electrons (Mn and Cu,[44,45] Ga[46,47] and Lu[48,49]). Metal basis sets were downloaded from the Basis Set Exchange website.[50–52] The integral equation formalism of the polarisable continuum model (IEFPCM) was used as an implicit water model in all calculations to simulate the average dielectric effects of the solvent. Default IEFPCM parameters were used, as implemented in Gaussian ($\varepsilon = 78.36$, van der Waals surface without "added spheres"). For Cu^{2+}–H_3glyox, calculations included 0, 1 and 3 explicit water molecules while for Mn just one explicit water molecule was included. Lu^{3+}–H_3glyox calculations included 2 explicit water molecules. Before optimisation, the randomly placed water molecules were placed closer to the metal with the aim to try to coordinate it to Cu^{2+}, Mn^{2+} or Lu^{3+} or to hydrogen bond centres, such as oxinates and carboxyl groups. Normal self-consistent field (SCF) and geometry convergence criteria were conducted for all the calculations. The calculated

structures were visualized using GaussView version 6.0 (ref. 53) and Avogadro version 1.2.0.[54]

Conflicts of interest

The authors declare no competing financial interest.

Acknowledgements

We gratefully acknowledge both the Canadian Institutes for Health Research (CIHR) and the Natural Sciences and Engineering Research Council (NSERC) of Canada for grant support, NSERC for an IsoSiM CREATE at TRIUMF studentship (NC), and MITACS for a Globalink Graduate fellowship (NC). We thank WestGrid and Compute Canada for access to their computational resources. Karin Landrock is acknowledged for excellent technical assistance, as is the HZDR for supporting the IsoSiM International Research Experience programme; TRIUMF receives federal funding *via* a contribution agreement with the National Research Council of Canada.

References

1 A. B. Garrett, *J. Chem. Educ.*, 1963, **40**, 36–37.
2 C. Hoehr, F. Bénard, K. Buckley, J. Crawford, A. Gottberg, V. Hanemaayer, P. Kunz, K. Ladouceur, V. Radchenko, C. Ramogida, A. Robertson, T. Ruth, N. Zacchia, S. Zeisler and P. Schaffer, *Phys. Procedia*, 2017, **90**, 200–208.
3 T. I. Kostelnik and C. Orvig, *Chem. Rev.*, 2019, **119**, 902–956.
4 E. Boros and A. B. Packard, *Chem. Rev.*, 2019, **119**, 870–901.
5 E. Boros and J. P. Holland, *J. Labelled Compd. Radiopharm.*, 2018, **61**, 652–671.
6 T. J. Wadas, E. H. Wong, G. R. Weisman and C. J. Anderson, *Chem. Rev.*, 2010, **110**, 2858–2902.
7 S. Sarkar, N. Bhatt, Y. S. Ha, P. T. Huynh, N. Soni, W. Lee, Y. J. Lee, J. Y. Kim, D. N. Pandya, G. Il An, K. C. Lee, Y. Chang and J. Yoo, *J. Med. Chem.*, 2018, **61**, 385–395.
8 P. Gawne, F. Man, J. Fonslet, R. Radia, J. Bordoloi, M. Cleveland, P. Jimenez-Royo, A. Gabizon, P. J. Blower, N. Long and R. T. M. De Rosales, *Dalton Trans.*, 2018, **47**, 9283–9293.
9 I. Verel, G. W. M. Visser, R. Boellaard, M. Stigter-van Walsum, G. B. Snow and G. A. M. S. van Dongen, *J. Nucl. Med.*, 2003, **44**, 1271–1281.
10 C. Vanasschen, M. Brandt, J. Ermert and H. H. Coenen, *Dalton Trans.*, 2016, **45**, 1315–1321.
11 E. M. Gale, I. P. Atanasova, F. Blasi, I. Ay and P. Caravan, *J. Am. Chem. Soc.*, 2015, **137**, 15548–15557.
12 F. K. Kálmán, F. K. Kálmán, V. Nagy, B. Váradi, Z. Garda, E. Molnár, G. Trencsényi, J. Kiss, S. Même, W. Même, É. Tóth and G. Tircsó, *J. Med. Chem.*, 2020, **63**, 6057–6065.
13 P. J. Blower, J. S. Lewis and J. Zweit, *Nucl. Med. Biol.*, 1996, **23**, 957–980.
14 S. Banerjee, M. R. A. Pillai and F. F. Knapp, *Chem. Rev.*, 2015, **115**, 2934–2974.
15 FDA approves lutetium Lu-177 dotatate for treatment of GEP-NETS, https://www.fda.gov/drugs/resources-information-approved-drugs/fda-approves-lutetium-lu-177-dotatate-treatment-gep-nets, accessed 13 July 2020.
16 N. Choudhary, M. d. G. Jaraquemada-Peláez, K. Zarschler, X. Wang, V. Radchenko, M. Kubeil, H. Stephan and C. Orvig, *Inorg. Chem.*, 2020, **59**, 5728–5741.
17 R. D. Shannon, *Acta Crystallogr., Sect. A: Cryst. Phys., Diffr., Theor. Gen. Crystallogr.*, 1976, **32**, 751–767.
18 G. K. Walkup and B. Imperiali, *J. Org. Chem.*, 1998, **63**, 6727–6731.
19 N. Choudhary, A. Dimmling, X. Wang, L. Southcott, V. Radchenko, B. O. Patrick, P. Comba and C. Orvig, *Inorg. Chem.*, 2019, **58**, 8685–8693.
20 D. Brox, A. Kiel, S. J. Wörner, M. Pernpointner, P. Comba, B. Martin and D. P. Herten, *PLoS One*, 2013, **8**, e58049.
21 L. Prodi, F. Bolletta, M. Montalti and N. Zaccheroni, *Coord. Chem. Rev.*, 2000, **205**, 59–83.
22 D. M. Weekes, C. F. Ramogida, M. d. G. Jaraquemada-Pelaez, B. O. Patrick, C. Apte, T. I. Kostelnik, J. F. Cawthray, L. Murphy and C. Orvig, *Inorg. Chem.*, 2016, **55**, 12544–12558.
23 X. Wang, M. d. G. Jaraquemada-Peláez, Y. Cao, J. Pan, K. S. Lin, B. O. Patrick and C. Orvig, *Inorg. Chem.*, 2019, **58**, 2275–2285.
24 A. Forgács, R. Pujales-Paradela, M. Regueiro-Figueroa, L. Valencia, D. Esteban-Gómez, M. Botta and C. Platas-Iglesias, *Dalton Trans.*, 2017, **46**, 1546–1558.
25 A. Pasquarello, I. Petri, P. S. Salmon, O. Parisel, R. Car, É. Tóth, D. H. Powell, H. E. Fischer, L. Helm and A. E. Merbach, *Science*, 2001, **291**, 856–859.
26 L. M. P. Lima, D. Esteban-Gómezgómez, R. Delgado, C. Platas-Iglesias and R. L. Tripier, *Inorg. Chem.*, 2012, **51**, 6916–6927.
27 B. A. Vaughn, A. M. Brown, S. H. Ahn, J. R. Robinson and E. Boros, *Inorg. Chem.*, 2020, **59**, 16095–16108.
28 X. Wang, *New Chelators for Radiopharmaceutical Chemistry, doctoral dissertation*, University of British Columbia, Vancouver, Canada, 2019.
29 A. Nonat, P. H. Fries, J. Pécaut and M. Mazzanti, *Chem.–Eur. J.*, 2007, **13**, 8489–8506.
30 P. Gans, A. Sabatini and A. Vacca, *Anal. Chim. Acta*, 1999, **89**, 45–49.
31 W. R. Harris, C. J. Carrano and K. N. Raymond, *J. Am. Chem. Soc.*, 1979, **101**, 2213–2214.
32 X. Wang, M. d. G. Jaraquemada-Peláez, C. Rodríguez-Rodríguez, Y. Cao, C. Buchwalder, N. Choudhary, U. Jermilova, C. F. Ramogida, K. Saatchi, U. Hafeli, B. O. Patrick and C. Orvig, *J. Am. Chem. Soc.*, 2018, **140**, 15487–15500.
33 B. Drahoš, J. Kotek, P. Hermann, I. Lukeš and É. Tóth, *Inorg. Chem.*, 2010, **49**, 3224–3238.
34 R. Botár, E. Molnár, G. Trencsényi, J. Kiss, F. K. Kálmán and G. Tircsó, *J. Am. Chem. Soc.*, 2020, **142**, 1662–1666.
35 K. E. Barrett, E. Aluicio-Sarduy, A. P. Olson, C. J. Kutyreff, P. A. Ellison, T. E. Barnhart, R. J. Nickles and J. W. Engle, *Appl. Radiat. Isot.*, 2019, **146**, 99–103.

36 D. Ndiaye, M. Sy, A. Pallier, S. Même, I. de Silva, S. Lacerda, A. M. Nonat, L. J. Charbonnière and É. Tóth, *Angew. Chem., Int. Ed.*, 2020, **59**, 11958–11963.
37 M. Kreller, H. Pietzsch, M. Walther, H. Tietze, P. Kaever, T. Knieß, F. Füchtner, J. Steinbach and S. Preusche, *Instruments*, 2019, **3**, 1–9.
38 M. d. G. Jaraquemada-Peláez, X. Wang, T. J. Clough, Y. Cao, N. Choudhary, K. Emler, B. O. Patrick and C. Orvig, *Dalton Trans.*, 2017, **46**, 14647–14658.
39 G. Gran, *Analyst*, 1952, **77**, 661–670.
40 C. F. Baes Jr and R. E. Mesmer, in *The Hydrolysis of Cations*, John Wiley & Sons, New York, 1976.
41 M. J. Frisch, G. W. Trucks, H. B. Schlegel, G. E. Scuseria, M. A. Robb, J. R. Cheeseman, G. Scalmani, V. Barone, G. A. Petersson, H. Nakatsuji, X. Li, M. Caricato, A. Marenich, J. Bloino, B. G. Janesko, R. Gomperts, B. Mennucci, H. P. Hratchian, J. V. Ortiz, A. F. Izmaylov, J. L. Sonnenberg, D. Williams-Young, F. Ding, F. Lipparini, F. Egidi, J. Goings, B. Peng, A. Petrone, T. Henderson, D. Ranasinghe, V. G. Zakrzewski, J. Gao, N. Rega, G. Zheng, W. Liang, M. Hada, M. Ehara, K. Toyota, R. Fukuda, J. Hasegawa, M. Ishida, T. Nakajima, Y. Honda, O. Kitao, H. Nakai, T. Vreven, K. Throssell, J. A. Montgomery Jr, J. E. Peralta, F. Ogliaro, M. Bearpark, J. J. Heyd, E. Brothers, K. N. Kudin, V. N. Staroverov, T. Keith, R. Kobayashi, J. Normand, K. Raghavachari, A. Rendell, J. C. Burant, S. S. Iyengar, J. Tomasi, M. Cossi, J. M. Millam, M. Klene, C. Adamo, R. Cammi, J. W. Ochterski, R. L. Martin, K. Morokuma, O. Farkas, J. B. Foresman and D. J. Fox, *Gaussian 09, Revision D.01*, Gaussian, Inc., Wallingford CT, 2016.
42 J. Tao, J. P. Perdew, V. N. Staroverov and G. E. Scuseria, *Phys. Rev. Lett.*, 2003, **91**, 146401.
43 F. Weigend and R. Ahlrichs, *Phys. Chem. Chem. Phys.*, 2005, **7**, 3297–3305.
44 M. Dolg, U. Wedig, H. Stoll and H. Preuss, *J. Chem. Phys.*, 1986, **86**, 866–872.
45 J. M. L. Martin and A. Sundermann, *J. Chem. Phys.*, 2001, **114**, 3408–3420.
46 T. Leininger, A. Berning, A. Nicklass, H. Stoll, H.-J. Werner and H.-J. Flad, *Chem. Phys.*, 1997, **217**, 19–27.
47 A. Bergner, M. Dolg, W. Küchle, H. Stoll and H. Preuß, *Mol. Phys.*, 1993, **80**, 1431–1441.
48 X. Cao and M. Dolg, *J. Chem. Phys.*, 2001, **115**, 7348–7355.
49 R. Gulde, P. Pollak and F. Weigend, *J. Chem. Theory Comput.*, 2012, **8**, 4062–4068.
50 K. L. Schuchardt, B. T. Didier, T. Elsethagen, L. Sun, V. Gurumoorthi, J. Chase, J. Li and T. L. Windus, *J. Chem. Inf. Model.*, 2007, **47**, 1045–1052.
51 B. P. Pritchard, D. Altarawy, B. Didier, T. D. Gibson and T. L. Windus, *J. Chem. Inf. Model.*, 2019, **59**, 4814–4820.
52 D. Feller, *J. Comput. Chem.*, 1996, **17**, 1571–1586.
53 R. Dennington, T. A. Keith and J. M. Millam, *GaussView, Version 6.0.16*, Semichem Inc., Shawnee Mission KS, 2016.
54 M. D. Hanwell, D. E. Curtis, D. C. Lonie, T. Vandermeerschd, E. Zurek and G. R. Hutchison, *J. Cheminf.*, 2012, **4**, 1–17.